ELSEVIER

Cell Calcium 41 (2007) 249–260

cell calcium

www.elsevier.com/locate/ceca

Cell cycle-dependent regulation of store-operated I_{CRAC} and Mg^{2+}-nucleotide-regulated MagNuM (TRPM7) currents

Dawn Tani [1], Mahealani K. Monteilh-Zoller [1], Andrea Fleig, Reinhold Penner *

Laboratory of Cell and Molecular Signaling, Center for Biomedical Research at The Queen's Medical Center and John A. Burns School of Medicine at the University of Hawaii, 1301 Punchbowl Street, UHT 8, Honolulu, HI 96813, USA

Received 11 April 2006; received in revised form 7 July 2006; accepted 7 July 2006
Available online 24 October 2006

Abstract

Calcium signaling is a central mechanism for numerous cellular functions and particularly relevant for immune cell proliferation. However, the role of calcium influx in mitotic cell cycle progression is largely unknown. We here report that proliferating rat mast cells RBL-2H3 tightly control their major store-operated calcium influx pathway, I_{CRAC}, during cell cycle progression. While I_{CRAC} is maintained at control levels during the first gap phase (G1), the current is significantly up-regulated in preparation for and during chromatin duplication. However, mitosis strongly suppresses I_{CRAC}. Non-proliferating cells deprived of growth hormones strongly down-regulate I_{CRAC} while increasing cell volume. We further show that the other known calcium (and magnesium) influx pathway in mast cells, the TRPM7-like magnesium-nucleotide-regulated metal (MagNuM) current, is largely uncoupled from cell cycle regulation except in G1. Taken together, our results demonstrate that both store-operated calcium influx via I_{CRAC} and MagNuM are regulated at crucial checkpoints during cell cycle progression.

Keywords: I_{CRAC}; MagNuM; TRPM7; Cell cycle

1. Introduction

Cell growth and division is a fundamental, tightly controlled process in the cell's life, whose deregulation can lead to pathological conditions [1]. A proliferating cell passes through an orderly sequence of phases that comprise the mitotic cell cycle: (i) gap phase 1 (G1), where cell mass grows and the cell prepares to synthesize DNA; (ii) synthesis phase (S), during which DNA synthesis occurs, duplicating the cell's genome; (iii) gap phase 2 (G2), in which DNA repair and protein synthesis prepare the cell's division; (iv) mitotic phase (M), in which division of the cell into two daughter cells takes place (cytokinesis) [2]. As the cell progresses through its cell phases, control is exerted at various checkpoints, during which the completion of the previous phase is ensured before the cell progresses to the next. These checkpoints involve various external or internal signals such as growth factors, substrate attachment of cells, and DNA repair activity. Currently known checkpoints are at the G1/S phase transition, the G2/M phase transition, and at the point of exit from mitosis [2].

Practically every eukaryotic organism uses Ca^{2+} as a ubiquitous second messenger inducing cellular events as diverse as allergic reactions, muscle contraction, transmitter release, or gene expression [3]. It comes as no surprise that the resumption and progression of the cell cycle, both mitotic and meiotic, seem to be accompanied by oscillatory changes in cytosolic Ca^{2+} [4,5]. Such Ca^{2+} signals are thought to be important in the late G1 phase, shortly before M, during M and during cytokinesis. For example, injection of Ca^{2+} chelators into fertilized sea urchin eggs was found to block the progression of the cycle, whereas Ca^{2+} ionophores induced its resumption [6,7]. Intracellular Ca^{2+} release triggers nuclear envelope breakdown and chromatin condensation in sea urchin eggs, fibroblasts, and in cultured animal cells [6–10]. Calcium transients have been characterized dur-

* Corresponding author. Tel.: +1 808 585 5366; fax: +1 808 585 5377.
E-mail address: rpenner@hawaii.edu (R. Penner).
[1] These authors contributed equally to this work.

0143-4160/$ – see front matter © 2006 Elsevier Ltd. All rights reserved.
doi:10.1016/j.ceca.2006.07.004

ing G1 and mitosis [11] and flow-cytometric studies indicate complex changes of Ca^{2+} levels throughout the mitotic division [12]. It is thought that Ca^{2+}-dependent proteins translate the Ca^{2+} signal into a molecular cascade of cellular responses [1]. Calmodulin, for example, is a Ca^{2+}-dependent cofactor that stimulates kinases, phosphatases, and proteases, all of which are important players in cell cycle control. In the example of proteases, the role of the Ca^{2+}-dependent enzyme calpain seems to be significant for cycle progression [13]. Several studies have explored the role of downstream calcium binding proteins such as calmodulin, calmodulin kinase II and calcineurin in mammalian cells [11]. The role of calcium and CaMII in re-initiating the meiotic cell cycle at fertilization is well documented [14] and the store-operated calcium current (SOC) in Xenopus oocytes is down-regulated during meiosis due to the activation of CDK1 [15,16].

Ca^{2+} homeostasis in RBL and Jurkat T cells is well documented [17]. The intricate interplay of several essential contributors determines cellular Ca^{2+} levels in these cells. Activation of cell surface receptors by growth factors, cytokines, mitogens, or antigen, induces inositol 1,4,5-trisphosphate ($InsP_3$) production and causes the release of Ca^{2+} from $InsP_3$-sensitive intracellular Ca^{2+} reservoirs [18,19]. Depleted Ca^{2+} stores, in turn, induce the activation of a selective Ca^{2+} influx pathway termed calcium release-activated calcium current (I_{CRAC}) [20]. Energy-driven Ca^{2+} pumps and transporters restore and maintain physiologically adequate Ca^{2+} concentrations in the cytosol. The physiological manifestation of these events lead to a wide range of Ca^{2+} signaling patterns that manifest themselves as single Ca^{2+} transients, repetitive oscillations, or sustained plateaus. These calcium signaling dynamics have been shown to act on gene expression [21,22]. I_{CRAC} is important for refilling of intracellular Ca^{2+} stores [23], modification of the spatio-temporal pattern of Ca^{2+} signaling [24], contribution to secretion [25], and regulation of enzymes like adenylate cyclase [26].

Given that Ca^{2+} influx plays an important role in cell proliferation, it is not surprising that ion channels have been implicated in regulating cell cycle progression. Changes in ion channel expression have been documented in some detail for potassium and chloride channels [27,28]. The former are thought to be important for setting the membrane potential and the driving force for Ca^{2+} influx and both are considered important for volume regulation of growing cells. Cell proliferation is regulated by a chain of events that begins with the interaction of growth factors with receptors located in the plasma membrane [29,30]. Ultimately, this leads to $InsP_3$ production, Ca^{2+} release and I_{CRAC} activation [17]. The role of Ca^{2+} store depletion and I_{CRAC} activation in cell cycle control is unknown. However, IL-2 production and lymphocyte proliferation are completely suppressed by removal of extracellular Ca^{2+} [31] or pharmacological block of I_{CRAC}. In addition, primary immunodeficiency, characterized by the inability to stimulate lymphocyte proliferation, has been linked to a genetic defect in I_{CRAC} [32,33]. Also, the phosphorylation of phosphoinositides by phosphatidylinositol-3-kinase is thought to play a crucial role in controlling cell proliferation [34]. It is tempting to speculate that Ca^{2+} release and I_{CRAC} are involved in the process.

TRPM7 is a ubiquitously expressed and constitutively active divalent cation channel, whose basal activity is regulated by intracellular levels of magnesium (Mg^{2+}) and Mg·ATP [35]. The channel permeates both Ca^{2+} and Mg^{2+} ions, but its ability to permeate Mg^{2+} is essential for cell growth and survival [36]. We previously described endogenous TRPM7-like Mg^{2+}-nucleotide-regulated metal currents (MagNuM) in RBL-2H3 cells [35,37]. Their contribution to cell cycle regulation is unknown, although recent data indicate a role of MagNuM in cell cycle progression at the G1/S border of retinoblastoma cells [38].

Little information is available on the effect of low extracellular Mg^{2+} on cell cycle [39]. Early work by Rubin suggested that Ca^{2+} and Mg^{2+} synergize in cell growth and proliferation [40]. Another group proposed that extracellular Mg^{2+} is essential for progression of WI-38 fibroblast from G1 into S phase [41]. This essential role of Mg^{2+} during the G1 phase was further strengthened by findings involving cyclins and cyclin-dependent kinases (CDK) [39]. Cyclins are positive regulators of CDKs that govern cell cycle progression in their complexed form. Cyclin-CDKs are under the control of inhibitory proteins belonging to the INK4 or Cip/Kip family. Specifically, the Cip/Kip family protein $p27^{kip1}$ inhibits CDKs responsible to push progression from G1 to S phase. Indeed, $p27^{kip1}$ is distinctively up-regulated in HL-60 and HC11 mammary epithelial cells grown in Mg^{2+}-deficient media [42,43] supporting the notion that the availability of extracellular Mg^{2+} during cell cycle progression is most important during G1.

We have carried out a number of experiments to characterize changes of I_{CRAC} and TRPM7-like MagNuM currents at various stages of the cell cycle in the rat mast cell line RBL-2H3. We performed patch-clamp experiments in the whole-cell configuration and measured DNA content by flow-cytometric population analyses. The current work shows that I_{CRAC} and MagNuM are tightly regulated at distinct cell cycle phases.

2. Methods

2.1. Cells

RBL-2H3-M1 cells were grown on glass coverslips with standard DMEM medium supplemented with 10% fetal bovine serum (FBS, Gibco) unless indicated otherwise (see below).

2.2. Flow cytometry using propidium iodine (PI) staining

PI staining was performed using established protocols [44]. Briefly, harvested RBL-2H3 cells were re-suspended in

a phosphate-buffered saline (PBS)/ethanol mixture (30/70%) and incubated in PBS containing 400 μg/ml PI (Sigma) and 1 mg/ml Rnase (Sigma). Samples were analyzed at The Queen's Medical Center Pathology Laboratory using a Coulter EPIC flow cytometer. Between 20,000 and 40,000 cells were analyzed per sample run. Results were gated to exclude doublets. Multicycle AV (Phoenix Flow Systems) was used as acquisition program and FlowJo (Tree Star, Inc.) and Igor Pro (WaveMetrics) were used for data analysis.

2.3. Synchronization of RBL-2H3-M1 cells in specific cell cycle phases

Synchronization was performed according to standard methods [45] and fine-tuned to RBL-2H3 cells. All protocols were designed to ensure that cells were both reversibly and almost completely arrested at one defined point in the cell cycle and confirmed by flow cytometry (FACS). The chemicals used to synchronize cells were tested acutely at a concentration of 10 μM on fully activated I_{CRAC} to ensure no direct effects (data not shown).

2.3.1. Synchronization in the G0-like and G1 phase using serum-, Ca^{2+}-, and isoleucine-deprivation

Exponentially growing cells were trypsinized, centrifuged, washed twice in sterile PBS and re-suspended at 30% of their confluent density (7.25×10^4 cells/ml) in medium that either contained 0% FBS, 20 μM $CaCl_2$ (standard medium with 1.348 mM K-Bapta added) or 0 mg/ml isoleucine (MEM Select Amine Kit, Invitrogen). For serum and isoleucine-deprivation cells were analyzed after 24 h by FACS and patch-clamp experiments. Cells that were Ca^{2+} deprived (20 μM) were analyzed 48 h by FACS and patch-clamp experiments.

2.3.2. Synchronization at the G1/S border

Cells were seeded and grown in isoleucine-free medium as described above. After 24 h cells were grown in standard medium with added 5 μg/ml aphidicolin (Sigma) for 8 h and analyzed by FACS. Patch-clamp experiments were performed at a maximum of 45 min per cover slip to avoid de-synchronization effects.

2.3.3. Synchronization in the middle of the S phase

Cells were grown in isoleucine-free conditions for 24 h and subsequently in aphidicoline conditions as described above for an additional 24 h. Cells were then released for 2 h in standard medium and growth-arrested using 2 mM thymidine block (Sigma) for 3 h before analysis.

2.3.4. Synchronization in G2

Cells were grown for 38 h in isoleucine-free medium and subsequently maintained in standard medium with 5 μg/ml aphidicolin for an additional 10 h. Cells were washed and returned into standard medium containing 500 ng/ml HOECHST 33342 (Sigma) for 8 h.

2.3.5. Synchronization in mitosis

Cells were grown until 60–80% confluency, tapped vigorously and the supernatant removed. The remaining cells were incubated in standard medium that contained 0.05 μg/ml nocodazole (Fluka) for 4 h. For patch-clamp experiments, harvested cells were kept in nocodazole containing medium in a 50 ml sterile tube on ice. About 500 μl of cells were removed from the tube, spun for 30 s in a picofuge, diluted in 500 μl external standard solution and plated on the experimental chamber. Cells were allowed to settle for 2 min before patch-clamping. Each mitotic plate thus prepared was used for a maximum of 45 min. Experiments were timed such that a new mitotic harvest was available after 4 h.

2.4. Solutions

Cells grown on glass coverslips were transferred to the recording chamber and kept in a standard modified Ringer's solution of the following composition (in mM): NaCl 140, KCl 2.8, $CaCl_2$ 10, $MgCl_2$ 2, glucose 11, Hepes·NaOH 10, pH 7.2. Intracellular pipette-filling solutions contained (in mM): Cs-glutamate 140, NaCl 8, $MgCl_2$ 1, Cs-BAPTA 10, 20 μM IP_3, 10 HEPES·CsOH, pH 7.2. Solution changes were performed by pressure ejection from a wide-tipped pipette to ascertain that the pharmaceuticals used in the cell cycle synchronization did not have any acute effects on I_{CRAC}.

2.5. Patch-clamp experiments

Patch-clamp experiments were performed in the tight-seal whole-cell configuration at 21–25 °C. High-resolution current recordings were acquired using the EPC-9 (HEKA). Voltage ramps of 50 ms duration spanning a range of −100 to +100 mV were delivered from a holding potential of 0 mV at a rate of 0.5 Hz over a period of 300–600 s. All voltages were corrected for a liquid junction potential of 10 mV. Currents were filtered at 2.9 kHz and digitized at 100 μs intervals. Capacitive currents were determined and corrected before each voltage ramp. Extracting the current amplitude at −80 mV for I_{CRAC} and +80 mV for MagNuM from individual ramp current records assessed the low-resolution temporal development of both currents. Where applicable, statistical errors of averaged data are given as means ± S.E.M. with *n* determinations. Gaussian, sigmoid and exponential curves were fitted using standard equations. Cell volume was calculated assuming spherical cell shape and a specific membrane capacitance of 1 μF/cm^2 [46].

3. Results

Continuously dividing cells maintain an exponential growth rate progressing through relatively well-defined

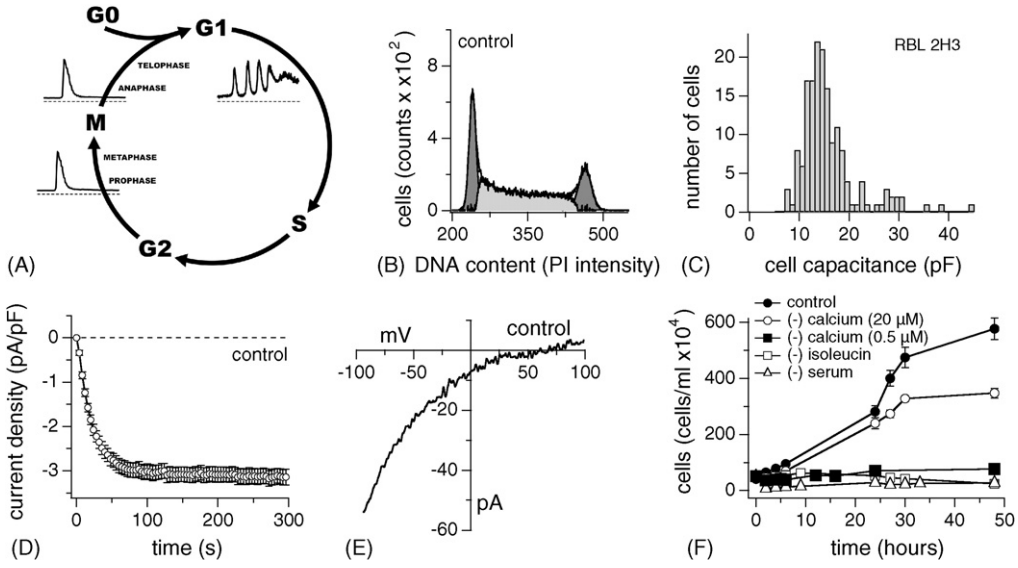

Fig. 1. Characteristics of I_{CRAC} in exponentially growing RBL-2H3 cells. (A) The cell cycle has distinct phases. Non-proliferating cells are in G0. Once a cell has been triggered to enter gap phase 1 (G1), division proceeds. This step seems to be dependent on the availability of extracellular Ca^{2+} and oscillations in $[Ca^{2+}]i$. So is the entrance into S phase. The S phase is followed by a short gap (G2) that finally leads to mitosis (M) and cell division. The availability of extracellular Ca^{2+} seems less important during distinct phases of mitosis and rather relies on single spikes of $[Ca^{2+}]i$ induced by $InsP_3$-induced Ca^{2+} release. (B) DNA profile of exponentially growing RBL-2H3 cells. The graph shows an example of exponentially grown RBL-2H3 cells subjected to propidium iodide (PI) staining and subsequent flow cytometry analysis (FACS; $n = 6$). The number of gated cells is plotted vs. PI intensity. The first peak indicates the DNA content of cells in G0/G1 and the second peak indicates cells in G2/M. Both peaks were fitted with Gaussian curves and the resulting integrals (dark grey areas) were subtracted from the DNA profile to arrive at the number of cells in S phase (light grey area). In this case 14,000 counts were acquired for analysis. (C) Cell surface of RBL-2H3 was estimated using the EPC-9's transient capacitance cancellation function, binned and plotted as a histogram ($n = 164$, grey bars, left ordinate). (D) Normalized average time course of I_{CRAC} activation measured in representative exponentially growing RBL-2H3. Currents of individual cells were measured at −80 mV, normalized by their respective cell size, averaged and plotted vs. time ($n = 42 \pm$ S.E.M.). (E) Leak-subtracted current–voltage (I/V) data trace of I_{CRAC} extracted at 100 s from an example cell. (F) Exponentially growing RBL-2H3 had a doubling time of about 4–10 h (filled circles). However, when subjected to serum-deprivation (open triangle, $n = 3$ each ± S.E.M.), isoleucine-deprivation (open square, $n = 3$ each ± S.E.M.) or Ca^{2+}-deprivation (20 μM Ca^{2+} open circle; 500 nM Ca^{2+} closed square; $n = 3$ each ± S.E.M., see Section 2) cell growth was arrested.

stages of the cell cycle. Progression into several of the cycle's phases involves $[Ca^{2+}]i$ signals of various forms, ranging from single spikes due to Ca^{2+} release to oscillations in Ca^{2+} caused by Ca^{2+} release and Ca^{2+} influx [47]. The various cell cycle stages and the changes in $[Ca^{2+}]i$ typically observed in oocytes and somatic cells [48] are illustrated schematically in Fig. 1A.

3.1. DNA profile, I_{CRAC} current density and cell capacitance of exponentially growing cells

Progression through the cell cycle is correlated with changes in both DNA content and cell capacitance [49]. We assessed these two parameters by flow cytometry (FACS) and patch-clamp measurements in RBL-2H3 cells. When grown under standard tissue culture conditions and populations are split regularly to avoid confluency, these cells maintain an exponential growth rate with a normal distribution between cell cycles (control conditions).

FACS takes advantage of the fact that DNA content doubles from G1 ($2n$) to M ($4n$), which is reflected by the emission intensity of propidium iodide (PI) bound to DNA. The results show that 38 ± 1.5% of cells were in G1, 41 ± 1.2% of cells were in the S phase, and 24 ± 2.7% of cells were in G2 or undergoing mitosis ($n = 6 \pm$ S.E.M., see Fig. 1B).

We next performed patch-clamp experiments to determine cell membrane capacitance, which represents a very accurate assessment of cell size, as it is directly correlated to cell surface area [50]. We assessed the capacitance of a large number of RBL-2H3 under control conditions (Fig. 1C) and determined an average value of 15.6 ± 0.31 pF ($n = 164$). However, the binned frequency distribution of cell capacitance values reveals that the cell size distribution is not uniformly Gaussian. Instead it is skewed, with the majority of cells being in the range of 11–16 pF (62%), about 20% of cells ranging from 17 to 20 pF, and the remaining cells being quite small (7 pF) or quite large (40 pF). This indicates that the majority of cells around 16 pF or less may reflect the dominant cell cycle stage of G1 and S, whereas the fewer large cells reflect cells in G2 and M phases.

Some of the cells analyzed for cell capacitance were also analyzed for the development of I_{CRAC} during the course of a whole-cell patch-clamp experiment. Using standard conditions, I_{CRAC} was measured in external sodium Ringer containing 10 mM Ca^{2+} and 10 mM Cs^+ to inhibit the inward-rectifier potassium channel. The cells were perfused intracellularly with a Cs-glutamate-based solution containing 10 mM BAPTA to chelate internal Ca^{2+} and 20 μM $InsP_3$ to fully release Ca^{2+} from intracellular stores. Voltage ramps of 50 ms duration and ranging from −100 to +100 mV were applied

every other second. Increases in inward currents were measured at −80 mV and plotted versus time (Fig. 1D; $n = 42$). A typical current–voltage data trace extracted at 100 s of whole-cell time is shown in Fig. 1E. The average peak inward current at −80 mV from the whole population was 3.16 ± 0.08 pA/pF ($n = 164 \pm$ S.E.M.).

3.2. Extracellular Ca^{2+} is crucial for cell cycle progression

Extracellular Ca^{2+} has long been implicated to play a role in cell cycle progression [47]. However, few studies have in fact investigated the effect of Ca^{2+}-deprivation on cell cycle [41,47,51–53]. WI-38 cells reportedly arrest in G1 if the Ca^{2+} in the medium falls below 60 μM [41]. We assessed the effects of lowering Ca^{2+} to 20 μM in the cell culture medium on the growth of RBL-2H3 cells and confirmed that under these conditions cells stop growing (Fig. 1F). FACS data (Fig. 2D, lower panel) indicate that 84 ± 1.7% ($n = 3$) were in G1, 7% in S and 6% in G2 or mitosis. However, growth arrest under 20 μM extracellular Ca^{2+} concentrations was somewhat slow and manifested itself after ∼48 h. Lowering extracellular Ca^{2+} even further (500 nM) prevented cell growth at start (Fig. 1F).

To study the properties of RBL cells at various defined cell cycle stages, we employed established protocols for arresting cells in desired phases. The agents in these protocols were selected for arresting cells at a single specific point in the cell cycle and the fact that their cell cycle block is reversible.

3.3. Serum withdrawal arrests RBL-2H3 cells in G0

A standard procedure to growth-arrest cells is to deprive them of serum for 24 h (see Section 2). This is thought to produce quiescent cells in G0, as it removes growth factors necessary to stimulate cell growth. In our hands, RBL-2H3 subjected to serum-deprivation indeed reacted with growth

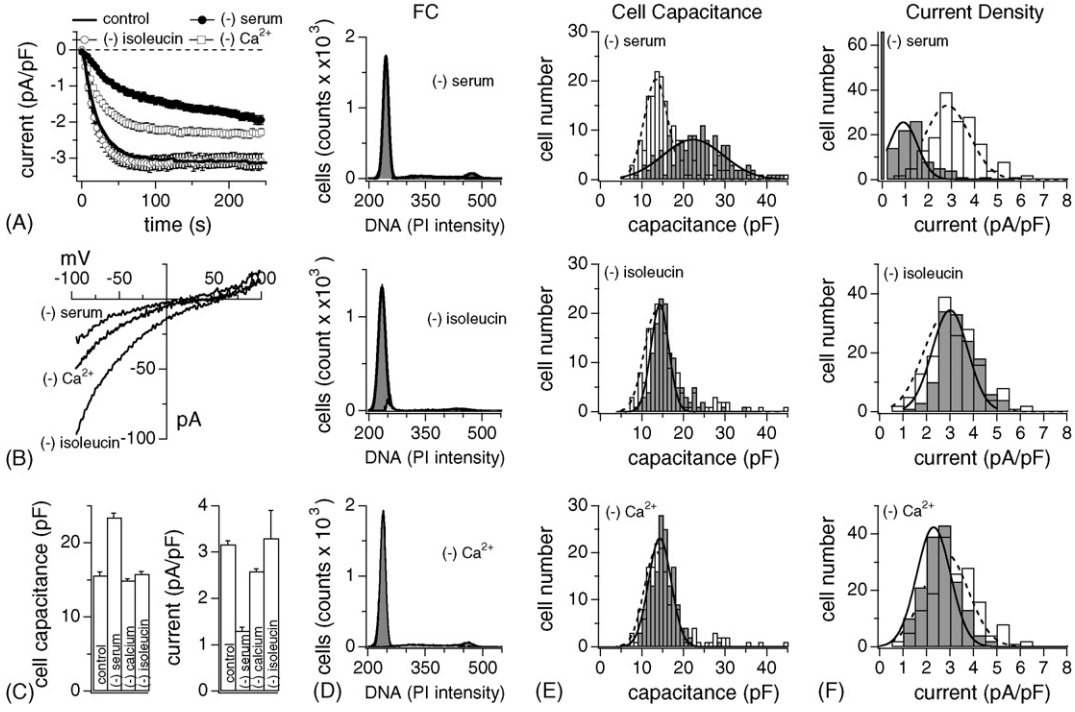

Fig. 2. G0/G1 arrest of RBL-2H3 cells by nutrient-deprivation induces differential effects on cell size and I_{CRAC}. (A) Normalized average time course of I_{CRAC} activation measured in RBL-2H3 growth-arrested by serum- (closed circle, $n = 82 \pm$ S.E.M.), isoleucine- (open circle, $n = 25 \pm$ S.E.M.) and extracellular Ca^{2+}-deprivation (20 μM, open square, $n = 34 \pm$ S.E.M.). Currents of individual cells were normalized by their respective cell size, averaged and plotted vs. time. (B) Leak-subtracted *I/V* data traces of I_{CRAC} extracted at 100 s from example cells exposed to nutrient-deprivation as indicated. (C) Average cell surface (left panel) and current density (right panel) of control ($n = 164$), serum- ($n = 148$), Ca^{2+}- ($n = 157$) and isoleucine-deprived RBL-2H3 ($n = 148$). Data ± S.E.M. (D) Examples of DNA profiles measured by FACS in RBL-2H3 subjected to serum- (upper panel; 75 ± 9% arrested in G0/G1, $n = 3$), isoleucine- (middle panel; 90 ± 1.7% arrested in G0/G1, $n = 2$) and Ca^{2+}-deprivation (lower panel; 94 ± 1.7% arrested in G0/G1, $n = 3$). Analysis as in Fig. 1B. (E) Nutrient-deprived RBL-2H3 (grey bars) and control cells (open bars) were analyzed for cell capacitance, binned, plotted and fitted with a Gaussian curve (dotted line for control cells, solid line for arrested cells). Cell surfaces were significantly larger than controls (open bars) and showed broad distribution in serum-deprived cells (upper panel). Isoleucine- (middle panel) and Ca^{2+}-deprivation (lower panel) had no significant effect on cell surface distribution compared to control (open bars). (F) Analysis of I_{CRAC} current densities of the same cells as in (E). The maximum current amplitude (in pA) was measured for each cell, normalized to cell capacitance (in pF). Cells were then binned according to current densities (open bars are control cells, grey bars represent deprived cells) and fitted with a Gaussian curve (dotted line for control cells, solid line for deprived cells). In serum-deprived cells about two thirds of the cells had significantly smaller I_{CRAC} than controls. One third of cells did not develop I_{CRAC} at all. Isoleucine-deprived cells had similar current densities to control cell (middle panel), however, Ca^{2+}-deprived cells were slightly smaller and skewed to the left (lower panel).

arrest as established by cell counting (Fig. 1F) and FACS (Fig. 2D). On average, 75 ± 9% of serum-deprived cells were arrested in G0 (Fig. 2D, upper panel, $n = 3$), with only 9 ± 3.7% in S and 9 ± 2.9% in G2 or mitosis. Another standard method of causing growth arrest is amino acid-deprivation in cycling cells. Omission of the amino acid isoleucine is most limiting to cells in mid-G1, about 4 h from the G1/S boundary [54]. Our results show that RBL-2H3 stopped growing very efficiently (Fig. 1F) with the majority of cells in G1 (90 ± 9%, Fig. 2D, middle panel, $n = 2$), and only 3 ± 0.2% in S and 4 ± 1.6% in G2 or mitosis.

We next assessed changes in cell size using these three methods for growth arrest. Cell capacitance values of 148 individual serum-deprived cells were pooled, binned, and plotted as a cell capacitance distribution histogram in Fig. 2E. Interestingly, serum-deprived cells had larger cell surfaces than control and had a wide distribution width as confirmed by the histogram plot (Fig. 2E, upper panel). In contrast, cells deprived of Ca^{2+} or isoleucine, were not enlarged and had cell size distributions very similar to control cells (Fig. 2E middle and lower panel).

Further analyses of the growth-arrested cells yielded estimates for activation time course (Fig. 2A) and peak current amplitudes of I_{CRAC} in individual RBL cells. To assess current densities, currents were normalized to cell capacitance (Fig. 2C and F). In general, serum-deprived cells had either no measurable or strongly reduced I_{CRAC} (Fig. 2A and C). The more detailed analysis using histogram plots (Fig. 2F) reveals that in serum-deprived conditions, 66 out of 148 cells did not express any discernible I_{CRAC} at all, and the rest had strongly suppressed currents. In contrast, Ca^{2+}- or isoleucine-deprivation had less or no effect on peak current densities (Fig. 2A and C).

3.4. I_{CRAC} increases in preparation for and during chromatin duplication

Inhibiting DNA synthesis using the DNA polymerase blocker aphidicolin reversibly arrests cells at the G1/S transition [45]. RBL-2H3 were first synchronized in G1 using 24-h isoleucin-deprivation and subsequently released into an aphidicolin-containing complete medium for 8 h (see Section 2). This efficiently arrested over 90% of cells at the G1/S transition (92 ± 2; S: 5 ± 1%; G2/M: 1.5 ± 0.4%; $n = 4$; Fig. 3A). During G1, cells start to increase in size as they produce proteins in preparation for DNA duplication. Indeed, when analyzing the membrane capacitance of individual cells, it is clear that cell surface at the G1/S border is significantly shifted to the right compared to control (Fig. 3B; average cell size = 21 ± 0.4 pF; $n = 149$). At the same time, I_{CRAC} also is significantly up-regulated, with the peak of the Gaussian distribution clearly shifted to the right (Fig. 3C; 4.4 ± 0.07 pA/pF; $n = 149$). Thus, I_{CRAC} is increased by about 40% compared to average values, consistent with the notion that the G1/S checkpoint is dependent on extracellular Ca^{2+} [41,51,52].

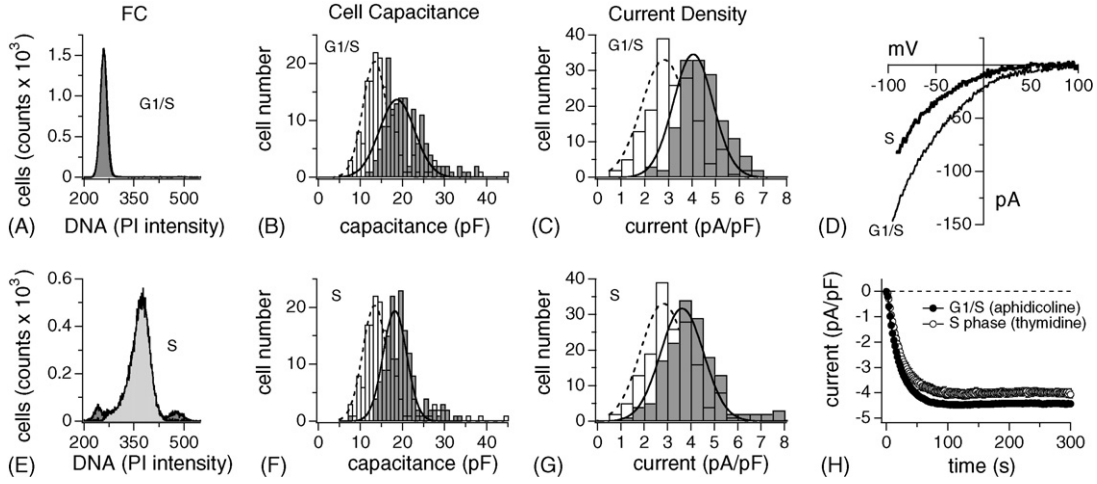

Fig. 3. Synchronization of RBL-2H3 cells in G1/S and S critically upregulates I_{CRAC}. (A) Example of a DNA profile measured by FACS in RBL-2H3 synchronized in G1/S using the aphidicolin protocol (see Section 2). About 92 ± 2% of cells arrested in G1/GS ($n = 4$). Analysis as in Fig. 1B. (B) Aphidicolin-arrested RBL-2H3 (grey bars) and control cells (open bars) were analyzed for cell capacitance, binned, plotted and fitted with a Gaussian curve (dotted line for control cells, solid line for arrested cells). Cell surfaces were significantly larger than controls (open bars) but showed a similar distribution width. (C) Analysis of I_{CRAC} current densities of the same cells as in (B) and as described in Fig. 2F. Current densities were clearly shifted to the right compared to control. Note that these cells are already normalized for cell capacitance, thus demonstrating a doubling of net I_{CRAC} at the G1/S border. (D) Leak-subtracted *I/V* data traces of I_{CRAC} extracted at 100 s from example cells at either the G1/S border or in the middle of the S phase, as indicated in the graph. (E) Example of a DNA profile measured by FACS in RBL-2H3 synchronized in the middle of the S phase using thymidine block (see Section 2). About 85 ± 2.2% of cells arrested in S ($n = 4$). Analysis as in Fig. 1B. (F) S phase-synchronized RBL-2H3 (grey bars) and control cells (open bars) were analyzed as described in (B). Cell surfaces were significantly larger than controls (open bars) but similar to G1/S border cells. (G) I_{CRAC} current densities of the same cells as in (F) and analyzed as described in Fig. 2F. Current densities were clearly shifted to the right compared to control but similar to the G1/S border. (H) Normalized average time course of I_{CRAC} activation measured in representative RBL-2H3 synchronized at the G1/S border (closed circle, $n = 38$ ± S.E.M.) and in S phase (open square, $n = 33$ ± S.E.M.). Current analysis as described in Fig. 2A.

We next set out to arrest the majority of cells in mid-S phase using a combination of isoleucine-deprivation, aphidicolin exposure, release of cells into S phase for 2 h and finally block by thymidine, a DNA synthesis inhibitor (see Section 2). This method reliably arrested 85 ± 2% in mid-S phase (Fig. 3E), with only 7 ± 0.6% of cells in G1 and 4 ± 1.6% of them in G2 or M (n = 4). The analysis of the cell capacitance and current density histograms (Fig. 3F and G) revealed that both parameters were comparable to the results obtained for the G1/S boundary. Both average cell size remained enlarged (20.5 ± 0.4 pF; n = 154) and I_{CRAC} stayed up-regulated (4 ± 0.09 pA/pF; n = 154). Importantly, the overall current–voltage relationship and time course of activation of I_{CRAC} did not change under these conditions (Fig. 3D and H).

To arrest cells in G2, where cells prepare for division, we adapted a well-established protocol that achieves efficient and reversible G2 synchronization using the topoisomerase II inhibitor HOECHST 33342 (see Section 2), rendering 70 ± 2% of cells in G2/M (Fig. 4A; G1: 14 ± 2%; S: 11 ± 2.3%; n = 5). As anticipated, cells had the largest cell surface at this stage of the cycle reaching up to 42 pF (Fig. 4B; n = 134) with a wide distribution profile. Furthermore, CRAC currents were still up-regulated, although a significant number of cells (29%) started to express normal or even smaller I_{CRAC} (Fig. 4C). It is important to note that the increase in I_{CRAC} reflects a genuine increase in current density that is not simply due to the change in cell size, since all the data have already been normalized to cell capacitance.

3.5. Mitotic RBL-2H3 cells regain normal cell volume but have strongly suppressed I_{CRAC}

We next set out to investigate the profile of cells collected in mitosis. Here, we took advantage of the drug nocodazole (see Section 2), which reversibly arrests cells at metaphase by destabilizing the microtubule structure [45]. Nocodazole synchronization successfully arrested 75 ± 5% of cells in metaphase (Fig. 4E; n = 3), with 6 ± 4% residing in G1 and 14 ± 3% of cells processing through S phase. Interestingly, when analyzing the cell capacitance histogram of 175 mitotic cells, it overlapped with the distribution measured in control cells (Fig. 4F). However, the current density profile for I_{CRAC} could be divided into three groups: 20% of cells expressed no I_{CRAC} at all, 43% had less than 1 pA/pF of current and the third group exhibited a Gaussian distribution peaking around 2.3 pA/pF. Averaging all cells rendered mitotic current densities at 1.25 ± 0.08 pA/pF (n = 175). The *I/V* relationship of I_{CRAC} (Fig. 4D) and its activation time course (Fig. 4H) were not affected by the mitotic cell cycle stage.

3.6. TRPM7-like MagNuM currents are uncoupled from cell cycle phases except during G1

Although mast cells employ store-operated Ca^{2+} influx as a major source for Ca^{2+} signaling following receptor stimulation, RBL-2H3 also possess homeostatic currents that regulate Ca^{2+} and Mg^{2+} transport. These are mediated by TRPM7 channels [35] and native currents that exhibit the TRPM7-

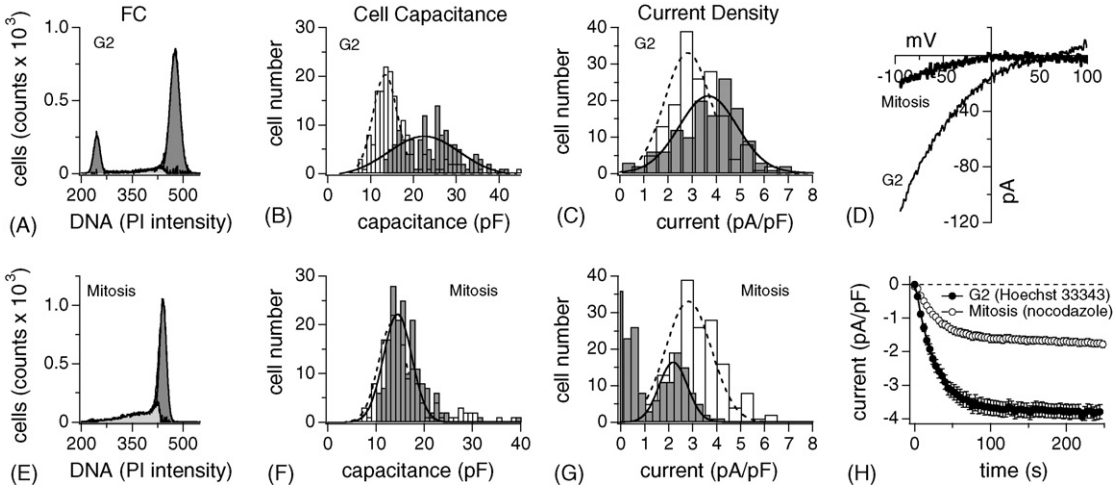

Fig. 4. Up-regulation of I_{CRAC} is maintained during G2 but drastically reduced in mitosis. (A) Example of a DNA profile measured by FACS in RBL-2H3 synchronized in G2 using HOECHST 33342 (see Section 2). On average, 70 ± 5% of cells arrested in G2 (n = 5). Analysis as in Fig. 1B. (B) G2-cells (grey bars) and control cells (open bars) were analyzed as described in Fig. 2E. Cell surfaces were at a maximum of all proliferation stages investigated (open bars) and showed a wide distribution. (C) Analysis of I_{CRAC} current densities of the same cells as in (B) and analyzed as described in Fig. 2F. Current densities were still shifted to the right compared to control but a significant portion of cells had already down-regulated their I_{CRAC}. (D) Leak-subtracted *I/V* data traces of I_{CRAC} extracted at 100 s from example cells at either the G2 stage or in mitosis, as indicated in the graph. (E) Example of a DNA profile measured by FACS in RBL-2H3 synchronized in mitosis (see Section 2). About 74 ± 5.2% of cells arrested in M (n = 3). Analysis as in Fig. 1C. (F) Mitosis-synchronized RBL-2H3 (grey bars) and control cells (open bars) were analyzed as described in Fig. 2E. Cell sizes had returned almost to normal. Note the absence of cells larger than 25 pF. (G) I_{CRAC} current densities of the same cells as in (F) and analyzed as described in Fig. 2F. I_{CRAC} is strongly down-regulated with many cells expressing no discernible Ca^{2+} influx at all. Note the distinct presence of two cell populations, one with little or no I_{CRAC}, the other with strongly suppressed I_{CRAC}. (H) Normalized average time course of I_{CRAC} activation measured in representative RBL-2H3 synchronized at G2 (closed circle, n = 40 ± S.E.M.) and in mitosis (open square, n = 76 ± S.E.M.). Current analysis as described in Fig. 2A.

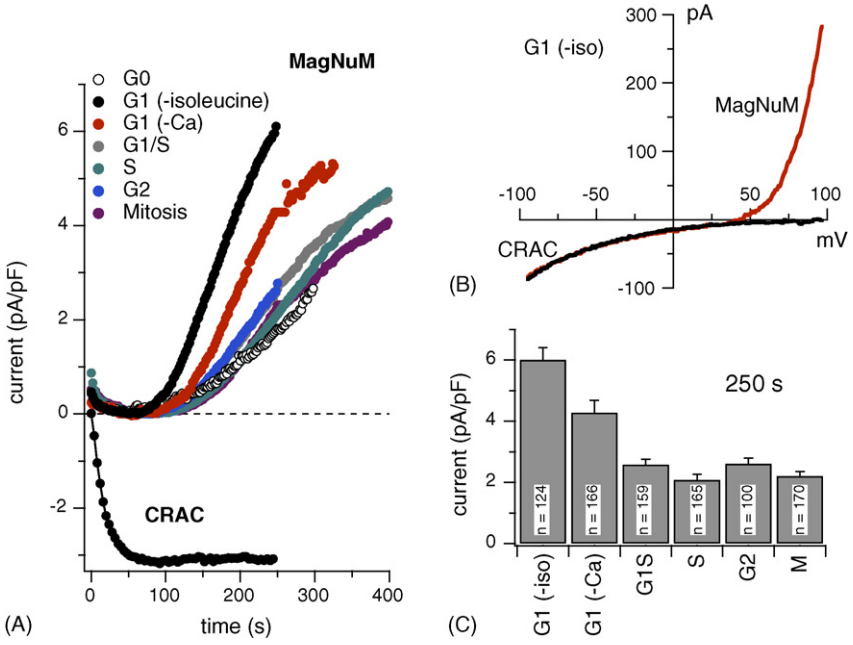

Fig. 5. TRPM7-like MagNuM currents do not significantly vary during cell cycle progression except at mid-G1. (A) Average time course of MagNuM activation at different cell cycle synchronization points. MagNuM currents of individual cells were measured at +80 mV, normalized by their respective cell size, averaged and plotted vs. time ($n = 100–170 \pm$ S.E.M.). Note the strong up-regulation of MagNuM in G1. The insert shows representative *I*/*V* relationships from a cell arrested in G1 by isoleucine-deprivation. The raw data trace for I_{CRAC} (black) was extracted after 50 s into the experiment. The combined raw data trace, where both MagNuM and I_{CRAC} can be measured at the same time, were extracted at 250 s into the experiment (red trace). Data were leak-corrected by subtracting the first voltage ramp measured after whole-cell break-in. (B) Current densities of MagNuM were measured at 250 s into the whole-cell experiment, averaged and plotted according to cell cycle progression. Proliferating cells overall expressed similar MagNuM except in G1, where currents are up-regulated by about 100%. (C) Current densities of I_{CRAC} were measured at 100 s into the experiment, averaged and plotted according to cell cycle progression. Note the up-regulation during G1/S, S and G2 and the strong down-regulation in M and G0.

specific inhibition by free $[Mg^{2+}]i$ and Mg-nucleotides have been characterized in T cells and RBL-2H3 and termed MagNuM [35,37]. MagNuM currents activate in RBL-2H3 under the experimental conditions typically used when studying I_{CRAC} [37] and they were also observed in the experiments of the present study as outwardly rectifying currents that develop slowly with a half-maximal current obtained at ~220 s, presumably due to omission of Mg·ATP from the pipette-filling solution. To gain insight on cell cycle-specific changes in MagNuM activity, we analyzed current records from the same cells analyzed for I_{CRAC} for possible changes in MagNuM current densities. This analysis was performed at +80 mV, where I_{CRAC} does not conduct significant outward currents. Fig. 5A illustrates the average time course and amplitudes of MagNuM currents for cells at the various stages and Fig. 5B shows the average current densities obtained at 250 s into the experiment. These data demonstrate that TRPM7 expression is tightly controlled across the cell cycle close to ~2 pA/pF of current density, irrespective of changes in cell size that occur. However, in mid-G1, the MagNuM current densities exhibit a near three-fold increase compared to all other stages (Fig. 5B). This observation is consistent for RBL-2H3 arrested in late G1 in low extracellular Ca^{2+} conditions. Here, the increase in current density is about two-fold. While the G1 stage exhibits normal I_{CRAC} densities, the MagNuM increase is dramatic and immediately returns to basal levels in subsequent stages, suggesting that both I_{CRAC} and MagNuM serve specific roles at specific cell cycle checkpoints.

4. Discussion

Signaling events involving Ca^{2+} release and Ca^{2+} influx are believed to be important factors in the complex regulation of cell growth and proliferation [47]. The present study underscores this notion in that the reduction of extracellular Ca^{2+} concentration indeed prevents RBL-2H3 cells from proliferating. Our results suggest that as these cells progress through the various stages of the cell cycle, they can up- or down-regulate ion channel pathways provided by the store-operated Ca^{2+} current I_{CRAC} and by the Mg^{2+}- and Mg^{2+}-nucleotide-regulated Ca^{2+}/Mg^{2+}-permeable ion current MagNuM (TRPM7). We find that I_{CRAC} current densities increase from normal levels of ~3 pA/pF (at −80 mV) in the G1 stage to ~4.5 pA/pF at the transition of G1/S phase and remain elevated throughout S and G2 phase until they precipitously fall to ~1 pA/pF during metaphase of mitosis. In contrast, MagNuM has a relatively stable current density of ~2 pA/pF (at +80 mV) in all stages, except for G1, where it is very high at ~6 pA/pF. This regulation appears to be specific for each of the pathways and suggests that it may be designed

to meet cellular demands for Ca^{2+} and/or Mg^{2+} fluxes of each cell stage.

We used established protocols to arrest cells at various cell cycle stages. Although most of the protocols involve some pharmacological manipulation, our results do not indicate that the observed effects were pharmacological in nature or unrelated to cell cycle arrest: (1) none of the treatments had any significant effect on I_{CRAC} or MagNuM when 10 μM of the individual compounds (aphidicoline, nocodazole, HOECHST 33342) was applied acutely after the currents were activated in control cells; (2) we never saw a concomitant suppression of CRAC and MagNuM currents that would indicate non-specific inhibition of ion channels by the pharmacological treatments or non-specific up- or down-regulation of ion channels in general; (3) we did not observe erratic up- or down-regulation of I_{CRAC} or MagNuM between adjacent cell cycle stages; (4) the amplitude distribution of I_{CRAC} in untreated, normally cycling cells is in excellent agreement with both the average amplitudes of cells arrested at individual cell cycle stages and their relative proportion within the mixed population of untreated cells.

While most of the treatments arrested ∼90% of the cells in the desired cell cycle stage, the arrest in G2 was somewhat less effective, resulting in 70% of cells in G2 and ∼15% in G1. Since the population of cells was not as uniform as in the other stages, the presence of a small population of cells in G1, which typically exhibit smaller cell surfaces and I_{CRAC}, may result in a slight underestimate of the G2-specific values. Nevertheless, we consider the data obtained for this stage as informative, since the average cell size was still largest compared to all other stages and I_{CRAC} amplitudes were still elevated. A similar non-uniform arrest of cells may affect the quantification of I_{CRAC} at mitosis. Based on FACS, we estimate that ∼75% of cells were in the mitotic stage and the rest in various stages leading up to it. The electrophysiology revealed contributions from two populations: one that had either no or very small I_{CRAC} below 1 pA/pF and a second population with amplitudes of ∼2 pA/pF, which may be due to the cells approaching but not yet arrested in metaphase. By averaging the current amplitudes of both populations, we may be slightly overestimating the true I_{CRAC} amplitude during mitosis itself and cells may in fact completely down-regulate I_{CRAC} during a narrow time frame within that stage.

The mitotic stage reveals another interesting phenomenon in that cells appear to have returned to normal capacitance of ∼15 pF as seen in G1, i.e., cell membrane capacitance is ∼50% of the cell surface achieved in G2, as if the cells had already divided. However, nocodazole arrests cells in metaphase by interfering with mitotic spindle formation, and would therefore rule out cell division as the reason for the capacitance decrease. It is thought that microtubules are essential in orchestrating the initiation of membrane retrieval in preparation for cytokinesis [55]. However, the whole-cell patch-clamp technique is the most sensitive approach to-date to measure minute changes in cells surface. Hence, this method may provide the ability to detect membrane retrieval at much earlier times than conventional fluorescent methods. Therefore, our data may indicate that a reduction in cell surface due to membrane retrieval in preparation for cell division may indeed start earlier in mitosis than previously assumed [55]. Such membrane retrieval may also engulf membrane proteins and could in part account for the reduction in I_{CRAC} we observe at this cell cycle stage. However, we do not see a significant decrease in the current density of MagNuM, suggesting that the process is not indiscriminate, but may involve specific membrane areas, possibly lipid rafts, that might predominantly harbor CRAC channels [56]. The overall reduction of I_{CRAC} and relative low abundance of MagNuM in mitotic cells indicates that Ca^{2+} influx plays a minor role during mitosis. This is in agreement with the observation that changes in intracellular Ca^{2+} levels during mitosis are predominantly due to $InsP_3$-induced Ca^{2+} release but not influx [13,19,57].

Another important aspect to consider is that the volume of the cell changes as well. Fig. 6 illustrates the cell cycle-dependent changes of both the cell surface as assessed by membrane capacitance and the corresponding cell volume, which was calculated assuming spherical shape of cells, a smooth unfolded cell surface and specific capacitance of 1 μF/cm^2 [46]. In terms of surface to volume ratio, this

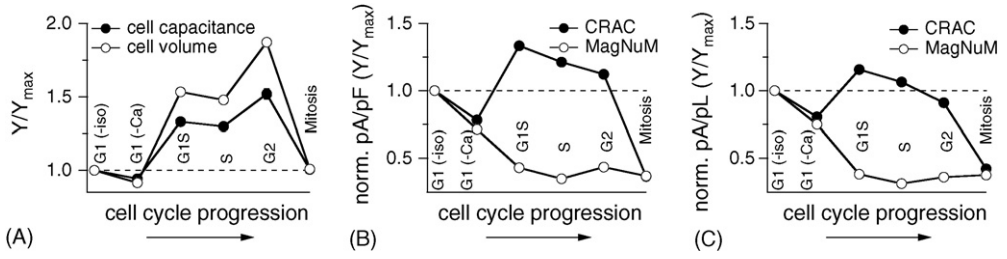

Fig. 6. Various cell cycle stages exhibit characteristic changes in cell size, cell volume I_{CRAC} and MagNuM. (A) Cell capacitances were averaged, normalized as Y/Y_{max} to the value obtained for isoleucine-deprived cells (G1(-iso)) and plotted vs. their respective cell cycle phase. Cell volume was calculated (see Section 2), normalized as Y/Y_{max} to G1(-iso) and plotted vs. cell cycle. (B) Cell cycle-specific current densities of I_{CRAC} (pA/pF; closed circles) measured at −80 mV and 100 s into the experiment were averaged, normalized as Y/Y_{max} to G1(-iso), and plotted vs. the respective phase. Current densities for MagNuM were measured at +80 mV and at 250 s experimental time, normalized to G1(-iso) and plotted vs. cell cycle stage. (C) The average current size (pA) of either I_{CRAC} (closed circles) or MagNuM (open circles) was divided by the calculated average cell volume (pL; see Section 2) for each respective cell cycle stage, normalized as Y/Y_{max} to G1(-iso) and plotted vs. cell cycle progression.

would mean that an x-fold increase in surface leads to an $x^{1.5}$-fold increase in volume. In both cases, the values of these parameters were normalized to those obtained at the isoleucine-induced G1 stage. As can be seen in Fig. 6A, the change in cell volume is even more dramatic than the change in surface area. Fig. 6B and C summarize the relative changes in I_{CRAC} and MagNuM as a function of cell surface and volume, respectively. This reveals that while the current density of I_{CRAC} is increased during S and G2 phases, it remains relatively constant when plotted against cell volume. This has functional consequences for store-operated Ca^{2+} influx in that the up-regulated I_{CRAC} will maintain its efficacy in providing the cytosol with relatively constant amounts of Ca^{2+} to change global $[Ca^{2+}]i$, however, the larger current densities will be more effective in regulating Ca^{2+}-dependent processes underneath the plasma membrane, in particular Ca^{2+}-dependent exocytosis, which represents a crucial physiological response of mast cells. During mitosis, I_{CRAC} is strongly down-regulated, suggesting that this process does not require significant contributions from store-operated mechanisms.

Our data also reveal an interesting regulation of I_{CRAC} by serum factors in that serum removal causes growth arrest in G0 and a massive down-regulation of I_{CRAC}. A previous study attributed this loss of I_{CRAC} to cell cycle arrest [58]. However, our data argue against a cell cycle-specific effect of serum-deprivation, since arresting cells at a similar, but proliferatively active stage does not cause I_{CRAC} reduction (Figs. 2 and 5C). Therefore, serum-deprivation appears to regulate I_{CRAC} independently of cell cycle stage, possibly through signal transduction mechanisms that control transcription factors needed for I_{CRAC} expression.

In contrast to I_{CRAC}, MagNuM is largest in G1 and is strongly down-regulated during cell growth, suggesting that its function as a Ca^{2+} and Mg^{2+} influx pathway is primarily needed during G1. It is presently unknown whether the function of MagNuM is based on its basal activity and simply provides a constant influx of Ca^{2+} and Mg^{2+} to maintain cellular homeostasis of these ions [35] or its activity is regulated by receptor signaling, as has been shown to be the case [59]. Although TRPM7/MagNuM have been clearly implicated in the regulation of cell growth [35,36,38], it remains to be determined what the relative roles of Ca^{2+} and Mg^{2+} transport through MagNuM are. We have previously demonstrated that supplementation of extracellular Mg^{2+}, but not Ca^{2+}, can restore cell growth in DT40 B cells in which TRPM7 has been knocked out [36], suggesting that Mg^{2+} transport is a crucial component of TRPM7 in supporting cell growth. On the other hand, Hanano et al. [38] have reported that the Ca^{2+} transport function of this channel may be important in regulating cell growth in retinoblastoma cells.

This effect may primarily influence the rate of proliferation, since siRNA-mediated knock down of TRPM7 delays the transition of cells from G1 into S phase. Furthermore, reports by Hazelton et al. [41] and work from Cittadini's group [42,43] emphasize the importance of extracellular Mg^{2+} specifically during G1 phase progression. Based on these and our data it is tempting to speculate that MagNuM, as a Ca^{2+}- and Mg^{2+}-permeable influx pathway, indeed provides these ions in a homeostatic fashion throughout G1, rendering the progression through this cell cycle stage largely independent of store-operated Ca^{2+} influx mediated by I_{CRAC}.

In summary, our data suggest that the two primary influx pathways for Ca^{2+}, I_{CRAC} and MagNuM, are regulated in characteristic manner as cells initiate proliferation. We determined that Ca^{2+} ions are a crucial component in driving cell proliferation, since Ca^{2+}-deprivation arrests cells in the G1 stage. The fact that this procedure traps cells in that particular stage would also suggest that Ca^{2+} influx is particularly important during that period of the cell cycle. Since MagNuM is up-regulated in that stage, we surmise that it might be an important factor in driving cell proliferation during G1. The down-regulation of MagNuM and the parallel up-regulation of I_{CRAC} in subsequent stages may reflect a shift in the requirements for Ca^{2+} influx, where the increased cell volume requires more effective store-dependent Ca^{2+} influx.

Acknowledgements

We thank The Queen's Medical Center Pathology Laboratory for the support in FACS acquisition and analysis. Financial support was provided by *The Queen Emma Research Foundation*, QERF-8021 and NIH R01-GM065360 to AF, and NIH R01-NS040927 and AI050200 to RP.

References

[1] J.F. Whitfield, R.P. Bird, B.R. Chakravarthy, R.J. Isaacs, P. Morley, Calcium-cell cycle regulator, differentiator, killer, chemopreventor, and maybe, tumor promoter, J. Cell. Biochem. Suppl. 22 (1995) 74–91.
[2] M. Pagano, Cell Cycle Control, Springer-Verlag, Berlin, Heidelberg, 1998.
[3] R. Penner, C. Fasolato, M. Hoth, Calcium influx and its control by calcium release, Curr. Opin. Neurobiol. 3 (1993) 368–374.
[4] A. Galione, H.C. Lee, W.B. Busa, Ca^{2+}-induced Ca^{2+} release in sea urchin egg homogenates: modulation by cyclic ADP-ribose, Science 253 (1991) 1143–1146.
[5] S. Miyazaki, M. Yuzaki, K. Nakada, H. Shirakawa, S. Nakanishi, S. Nakade, K. Mikoshiba, Block of Ca^{2+} wave and Ca^{2+} oscillation by antibody to the inositol 1,4,5-trisphosphate receptor in fertilized hamster eggs, Science 257 (1992) 251–255.
[6] R.S. Zucker, R.A. Steinhardt, Prevention of the cortical reaction in fertilized sea urchin eggs by injection of calcium-chelating ligands, Biochim. Biophys. Acta 541 (1978) 459–466.
[7] R.S. Zucker, R.A. Steinhardt, M.M. Winkler, Intracellular calcium release and the mechanisms of parthenogenetic activation of the sea urchin egg, Dev. Biol. 65 (1978) 285–295.
[8] J.P. Kao, J.M. Alderton, R.Y. Tsien, R.A. Steinhardt, Active involvement of Ca^{2+} in mitotic progression of Swiss 3T3 fibroblasts, J. Cell Biol. 111 (1990) 183–196.
[9] M. Poenie, J. Alderton, R. Steinhardt, R. Tsien, Calcium rises abruptly and briefly throughout the cell at the onset of anaphase, Science 233 (1986) 886–889.

[10] M. Poenie, J. Alderton, R.Y. Tsien, R.A. Steinhardt, Changes of free calcium levels with stages of the cell division cycle, Nature 315 (1985) 147–149.
[11] C.R. Kahl, A.R. Means, Regulation of cell cycle progression by calcium/calmodulin-dependent pathways, Endocr. Rev. 24 (2003) 719–736.
[12] G. Pande, N.A. Kumar, P.S. Manogaran, Flow cytometric study of changes in the intracellular free calcium during the cell cycle, Cytometry 24 (1996) 55–63.
[13] L. Santella, The role of calcium in the cell cycle: facts and hypotheses, Biochem. Biophys. Res. Commun. 244 (1998) 317–324.
[14] M. Whitaker, Calcium at fertilization and in early development, Physiol. Rev. 86 (2006) 25–88.
[15] K. Machaca, S. Haun, Store-operated calcium entry inactivates at the germinal vesicle breakdown stage of Xenopus meiosis, J. Biol. Chem. 275 (2000) 38710–38715.
[16] K. Machaca, S. Haun, Induction of maturation-promoting factor during Xenopus oocyte maturation uncouples Ca^{2+} store depletion from store-operated Ca^{2+} entry, J. Cell Biol. 156 (2002) 75–85.
[17] A.B. Parekh, R. Penner, Store depletion and calcium influx, Physiol. Rev. 77 (1997) 901–930.
[18] M.J. Berridge, Calcium oscillations, J. Biol. Chem. 265 (1990) 9583–9586.
[19] B. Ciapa, D. Pesando, M. Wilding, M. Whitaker, Cell-cycle calcium transients driven by cyclic changes in inositol trisphosphate levels, Nature 368 (1994) 875–878.
[20] M. Hoth, R. Penner, Depletion of intracellular calcium stores activates a calcium current in mast cells, Nature 355 (1992) 353–386.
[21] S. Feske, J. Giltnane, R. Dolmetsch, L.M. Staudt, A. Rao, Gene regulation mediated by calcium signals in T lymphocytes, Nat. Immunol. 2 (2001) 316–324.
[22] R.E. Dolmetsch, K. Xu, R.S. Lewis, Calcium oscillations increase the efficiency and specificity of gene expression, Nature 392 (1998) 933–936.
[23] A.B. Parekh, M. Foguet, H. Lübbert, W. Stühmer, Ca^{2+} oscillations and Ca^{2+} influx in Xenopus oocytes expressing a novel 5-hydroxytryptamine receptor, J. Physiol. (Lond.) 469 (1993) 653–671.
[24] S. Girard, D. Clapham, Acceleration of intracellular calcium waves in Xenopus oocytes by calcium influx, Science 260 (1993) 229–232.
[25] A.B. Parekh, R. Penner, Activation of store-operated calcium influx at resting $InsP_3$ levels by sensitization of the $InsP_3$ receptor in rat basophilic leukaemia cells, J. Physiol. (Lond.) 489 (Pt. 2) (1995) 377–382.
[26] M. Chiono, R. Mahey, G. Tate, D.M. Cooper, Capacitative Ca^{2+} entry exclusively inhibits cAMP synthesis in C6-2B glioma cells. Evidence that physiologically evoked Ca^{2+} entry regulates $Ca^{(2+)}$-inhibitable adenylyl cyclase in non-excitable cells, J. Biol. Chem. 270 (1995) 1149–1155.
[27] K. Kunzelmann, Ion channels and cancer, J. Membr. Biol. 205 (2005) 159–173.
[28] W.F. Wonderlin, J.S. Strobl, Potassium channels, proliferation and G1 progression, J. Membr. Biol. 154 (1996) 91–107.
[29] D.N. Brindley, D.W. Waggoner, Phosphatidate phosphohydrolase and signal transduction, Chem. Phys. Lipids 80 (1996) 45–57.
[30] D.L. Cadena, G.N. Gill, Receptor tyrosine kinases, FASEB J. 6 (1992) 2332–2337.
[31] H. Komada, H. Nakabayashi, M. Hara, K. Izutsu, Early calcium signaling and calcium requirements for the IL-2 receptor expression and IL-2 production in stimulated lymphocytes, Cell. Immunol. 173 (1996) 215–220.
[32] M. Partiseti, F. Le Deist, C. Hivroz, A. Fischer, H. Korn, D. Choquet, The calcium current activated by T cell receptor and store depletion in human lymphocytes is absent in a primary immunodeficiency, J. Biol. Chem. 269 (1994) 32327–32335.
[33] S. Feske, M. Prakriya, A. Rao, R.S. Lewis, A severe defect in CRAC Ca^{2+} channel activation and altered K^+ channel gating in T cells from immunodeficient patients, J. Exp. Med. 202 (2005) 651–662.
[34] A. Klippel, M.A. Escobedo, M.S. Wachowicz, G. Apell, T.W. Brown, M.A. Giedlin, W.M. Kavanaugh, L.T. Williams, Activation of phosphatidylinositol 3-kinase is sufficient for cell cycle entry and promotes cellular changes characteristic of oncogenic transformation, Mol. Cell. Biol. 18 (1998) 5699–5711.
[35] M.J. Nadler, M.C. Hermosura, K. Inabe, A.L. Perraud, Q. Zhu, A.J. Stokes, T. Kurosaki, J.P. Kinet, R. Penner, A.M. Scharenberg, A. Fleig, LTRPC7 is a Mg·ATP-regulated divalent cation channel required for cell viability, Nature 411 (2001) 590–595.
[36] C. Schmitz, A.L. Perraud, C.O. Johnson, K. Inabe, M.K. Smith, R. Penner, T. Kurosaki, A. Fleig, A.M. Scharenberg, Regulation of vertebrate cellular Mg^{2+} homeostasis by TRPM7, Cell 114 (2003) 191–200.
[37] M.C. Hermosura, M.K. Monteilh-Zoller, A.M. Scharenberg, R. Penner, A. Fleig, Dissociation of the store-operated calcium current I_{CRAC} and the Mg-nucleotide-regulated metal ion current MagNuM, J. Physiol. (Lond.) 539 (2002) 445–458.
[38] T. Hanano, Y. Hara, J. Shi, H. Morita, C. Umebayashi, E. Mori, H. Sumimoto, Y. Ito, Y. Mori, R. Inoue, Involvement of TRPM7 in cell growth as a spontaneously activated Ca^{2+} entry pathway in human retinoblastoma cells, J. Pharmacol. Sci. 95 (2004) 403–419.
[39] F.I. Wolf, A. Cittadini, Magnesium in cell proliferation and differentiation, Front. Biosci. 4 (1999) D607–D617.
[40] A.H. Rubin, M. Terasaki, H. Sanui, Magnesium reverses inhibitory effects of calcium deprivation on coordinate response of 3T3 cells to serum, Proc. Natl. Acad. Sci. U.S.A. 75 (1978) 4379–4383.
[41] B. Hazelton, B. Mitchell, J. Tupper, Calcium, magnesium, and growth control in the WI-38 human fibroblast cell, J. Cell Biol. 83 (1979) 487–498.
[42] V. Covacci, N. Bruzzese, A. Sgambato, A. Di Francesco, M.A. Russo, F.I. Wolf, A. Cittadini, Magnesium restriction induces granulocytic differentiation and expression of $p27^{Kip1}$ in human leukemic HL-60 cells, J. Cell. Biochem. 70 (1998) 313–322.
[43] A. Sgambato, F.I. Wolf, B. Faraglia, A. Cittadini, Magnesium depletion causes growth inhibition, reduced expression of cyclin D1, and increased expression of $P27^{Kip1}$ in normal but not in transformed mammary epithelial cells, J. Cell. Physiol. 180 (1999) 245–254.
[44] S. Verhaegen, S. Coyle, L.M. Connolly, C. O'Loughlin, M. Clynes, Analysis of cell cycle and cell death mechanisms, in: M. Clynes (Ed.), Animal Cell Culture Techniques, Springer, Berlin, 1998, pp. 170–193.
[45] W. Krek, J.A. DeCaprio, Cell synchronization, Meth. Enzymol. 254 (1995) 114–124.
[46] K.S. Cole, Membranes, Ions and Impulses: A Chapter of Classical Biophysics, University of California Press, Los Angeles, London, 1968.
[47] R. Schreiber, Ca^{2+} signaling, intracellular pH and cell volume in cell proliferation, J. Membr. Biol. 205 (2005) 129–137.
[48] M. Whitaker, R. Patel, Calcium and cell cycle control, Development 108 (1990) 525–542.
[49] D.L. Spector, R.D. Goldman, L.A. Leinwand, Cells. A Laboratory Manual, Cold Spring Harbor Laboratory Press, 1998.
[50] E. Neher, A. Marty, Discrete changes of cell membrane capacitance observed under conditions of enhanced secretion in bovine adrenal chromaffin cells, Proc. Natl. Acad. Sci. U.S.A. 79 (1982) 6712–6716.
[51] A.L. Boynton, J.F. Whitfield, R.J. Isaacs, The different roles of serum and calcium in the control of proliferation of BALB/c 3T3 mouse cells, In Vitro 12 (1976) 120–123.
[52] A.L. Boynton, J.F. Whitfield, R.J. Isaacs, R. Tremblay, The control of human WI-38 cell proliferation by extracellular calcium and its elimination by SV-40 virus-induced proliferative transformation, J. Cell. Physiol. 92 (1977) 241–247.
[53] I. Kojima, H. Mogami, H. Shibata, E. Ogata, Role of calcium entry and protein kinase C in the progression activity of insulin-like growth factor-I in Balb/c 3T3 cells, J. Biol. Chem. 268 (1993) 10003–10006.
[54] J.A. DeCaprio, J.W. Ludlow, D. Lynch, Y. Furukawa, J. Griffin, H. Piwnica-Worms, C.M. Huang, D.M. Livingston, The product of the retinoblastoma susceptibility gene has properties of a cell cycle regulatory element, Cell 58 (1989) 1085–1095.

[55] A.F. Straight, C.M. Field, Microtubules, membranes and cytokinesis, Curr. Biol. 10 (2000) R760–R770.
[56] N.F. Neel, E. Schutyser, J. Sai, G.H. Fan, A. Richmond, Chemokine receptor internalization and intracellular trafficking, Cytokine Growth Factor Rev. 16 (2005) 637–658.
[57] M. Sugioka, M. Yamashita, Calcium signaling to nucleus via store-operated system during cell cycle in retinal neuroepithelium, Neurosci. Res. 45 (2003) 447–458.
[58] M. Bodding, Reduced store-operated Ca^{2+} currents in rat basophilic leukaemia cells cultured under serum-free conditions, Cell Calcium 30 (2001) 141–150.
[59] R. Takezawa, C. Schmitz, P. Demeuse, A.M. Scharenberg, R. Penner, A. Fleig, Receptor-mediated regulation of the TRPM7 channel through its endogenous protein kinase domain, Proc. Natl. Acad. Sci. U.S.A. 101 (2004) 6009–6014.